

FlowPool: Pooling Graph Representations with Wasserstein Gradient Flows

Effrosyni Simou

Abstract

In several machine learning tasks for graph structured data, the graphs under consideration may be composed of a varying number of nodes. Therefore, it is necessary to design pooling methods that aggregate the graph representations of varying size to representations of fixed size which can be used in downstream tasks, such as graph classification. Existing graph pooling methods offer no guarantee with regards to the similarity of a graph representation and its pooled version. In this work we address this limitation by proposing FlowPool, a pooling method that optimally preserves the statistics of a graph representation to its pooled counterpart by minimizing their Wasserstein distance. This is achieved by performing a Wasserstein gradient flow with respect to the pooled graph representation. We propose a versatile implementation of our method which can take into account the geometry of the representation space through any ground cost. This implementation relies on the computation of the gradient of the Wasserstein distance with recently proposed implicit differentiation schemes. Our pooling method is amenable to automatic differentiation and can be integrated in end-to-end deep learning architectures. Further, FlowPool is invariant to permutations and can therefore be combined with permutation equivariant feature extraction layers in GNNs in order to obtain predictions that are independent of the ordering of the nodes. Experimental results demonstrate that our method leads to an increase in performance compared to existing pooling methods when evaluated in graph classification tasks.

1 Introduction

In machine learning problems, such as graph classification or graph regression, each datapoint corresponds to a different graph. Examples of such problems arise in the fields of computational biology, drug discovery and social network analysis, among others. For instance, a task of interest is the prediction of whether a protein structure is an enzyme or not. In that case, proteins are represented as graphs with nodes corresponding to amino-acids and edges capturing the spatial proximity of the amino-acids. Similarly, molecules can be represented as graphs where nodes are atoms and edges the chemical bonds between them. The problem of interest in that case may be the classification of a molecule as active or inactive against cancer cells.

Such tasks are tackled by models that operate in an inductive setting. In this setting, the goal of graph representation learning algorithms is to use a set of k training graphs G_1, \dots, G_k in order to learn a mapping that can generalize to unseen test graphs G_{k+1}, \dots, G_{k+l} . Naturally, the graphs can be of varying size. For instance, in the example of molecule classification discussed above, each molecule may be composed of a different number of atoms. As a result, a relevant problem that arises in Graph Neural Network (GNN) architectures in this context, is to find the optimal way to pool the graph representations of varying size to a representation of fixed size that can be multiplied by the weights of the classifier or regressor that is driving the representation learning process. This operation is commonly referred to as global graph pooling.

Graph pooling methods proposed fall into two categories: node selection methods and node clustering methods. Node selection methods aim to pool graph representations by selecting the representations of the most important nodes of the graph, according to some criterion. An important disadvantage of these methods is that they discard the information that is captured in the representations of the least important nodes. Node clustering methods propose to pool graph representations by learning node assignment matrices. The motivation of these methods is to learn what constitutes nodes to

be similar, so that the representations of similar nodes can be linearly combined, as dictated by the assignment matrices. Node clustering methods don't discard information, but aggregate the representations of similar nodes. However they still offer no guarantee with regards to the similarity of the graph representation and its pooled version.

In this work ¹, we introduce a new type of pooling method, that addresses this limitation. We propose to explicitly preserve the statistics of the graph representation by minimizing the entropy-regularized Wasserstein distance between itself and its pooled version. Our pooling method minimizes this distance by performing a Wasserstein gradient flow with respect to the pooled graph representation. Therefore, we term our proposed pooling method FlowPool. At each step of the flow, the energy of the Wasserstein distance between the graph representation and its pooled counterpart is computed and the pooled representation is moved closer to the original graph representation according to the gradient of that energy. As a result, the pooled graph representation, obtained with FlowPool, combines the representations of the nodes using the optimal couplings that minimize the Wasserstein distance along the steps of the flow.

Our contributions in this work are threefold:

- We propose a global pooling framework for graphs that optimally preserves the statistics in the representation space.
- We propose a versatile implementation of this pooling method using implicit differentiation [1] that can take into account any underlying geometry and that enables its integration in end-to-end deep learning architectures for graphs.
- We analyse the proposed pooling method for the case where the geometry considered is that determined by the squared Euclidean distance in the feature space and provide promising results for graph classification on real data.

The structure of this article is as follows. First, in Section 2 we review the related work. Further, in Section 3 we present preliminaries from Optimal Transport theory [2], [3] that are necessary to the comprehension of the proposed pooling method. After introducing the correspondence of a graph representation to a probability measure in Section 4, we propose FlowPool as the minimization of the Wasserstein distance between graph representations in Section 5. In Section 6 we explain our versatile implementation based on implicit automatic differentiation that can be used with any ground cost. In Section 7 we show that our method is invariant to permutations. In Section 8 we discuss how we can backpropagate through FlowPool and integrate it in end-to-end GNN architectures. In Section 9.1 we perform an experimental analysis for a simplified set-up of FlowPool in order to show its dependence on parameters and build intuitions and in Section 9.2 we provide preliminary results on graph classification when FlowPool is incorporated in an end-to-end deep learning architecture. We provide direction for future work in Section 10 and conclude in Section 11.

2 Related Work

As mentioned before, existing pooling methods for graphs can be grouped into two categories, namely node selection methods and node clustering methods. We review briefly representative methods from each of these two categories.

Node selection methods pool a graph representation by keeping only the representations of the K most important nodes in the graph. The first node selection method proposed is SortPool [4], which extends the idea of the Weisfeiler-Lehman graph kernels [5] to sort nodes based on their color, to sorting nodes based on their GCN feature vector. Once the nodes have been sorted, only the K most important ones are kept. Sortpool yields the same representation for isomorphic graphs. A different approach is followed by TopKPool [6]. TopKPool proposes to learn from the data a vector of parameters, such that only the K node representations, whose inner product with the trainable vector is maximal, are kept.

¹The content of this article corresponds to a chapter included in the PhD thesis submitted on September 10th 2021 and successfully defended on October 15th 2021. The thesis manuscript will be published online by EPFL the day after its presentation at the PhD graduation ceremony.

TopKPool does not explicitly take into account the graph structure. This limitation is addressed by SAGPool [7]. SAGPool employs a trainable graph convolutional layer in order to obtain an attention score for each node in the graph, and keeps only the K nodes that correspond to the highest attention scores.

Node selection methods lead to loss of information due to the discarded features of the nodes that are not selected. Node clustering methods aim to alleviate this problem by finding the optimal way to aggregate the representations of all N nodes in a graph. This is achieved by clustering the N nodes into M clusters in order to obtain an $N \times M$ assignment matrix S . As a result, given a graph of N nodes with adjacency matrix A and a $d \times N$ graph representation Y , the representation output by node clustering pooling methods is equal to $X = YS$. Further, the assignment matrix S provides a way to obtain the adjacency matrix A_c of the pooled graph as $A_c = S^T A S$. All proposed node clustering methods learn the assignment matrices from the data in order to achieve statistical strength. We provide a summary of existing node clustering pooling methods below.

The first differentiable graph pooling method that proposes to learn assignment matrices is DiffPool [8]. DiffPool proposes to parametrize node assignment matrices with a graph convolutional filter followed by a softmax activation. The parameters of the GCN filter are learned from the data during training. Therefore, DiffPool’s assignment matrices learn which nodes should be grouped together, based on the features and the graph structure. Building on DiffPool’s concept of parametrizing assignment matrices with GCNs, StructPool [9] proposes to condition the cluster assignment of each node on the cluster assignments of other nodes. As a result, the graph pooling problem is framed as a structured prediction problem by employing conditional random fields to capture the relationships among the assignments of the nodes. On a different line, HaarPool [10] employs the Haar basis [11], [12] matrix to obtain a mapping of the nodes in the graph to the nodes of the pooled graph. The graph is pooled by keeping the basis vectors that correspond to the low frequencies, thus maintaining the coarse structural information, and discarding the ones that correspond to the high frequencies, thus dismissing fine structural information. In order to leverage the node features as well as the spectral information of the graph structure, MinCutPool [13] proposes to parametrize node assignment matrices using multi-layer perceptrons and adds a term at the objective function which is a relaxation of the normalized minCUT problem [14].

Graph pooling is employed in deep networks for graph representation learning in two different contexts; hierarchical pooling and global pooling. Hierarchical pooling aims to generalize the pooling operation, as performed in convolutional networks for regular grids, and aggregate feature information over local patches in order to achieve locality-preserving representations and invariance to small deformations. Global pooling aims to learn fixed-size representations from graph representations of varying size. In a recent study [15] it is demonstrated that certain graph pooling methods, when employed for hierarchical pooling, do not enhance the graph representation learning process, but rather smooth the features of the nodes in the pooled graph representation. Although in this work we focus on global graph pooling, we mention that our proposed pooling method can also be used for hierarchical pooling and that it could help alleviate the smoothing problem because of the explicit objective of preserving the statistics. In that context, the coarsened graph adjacency matrix A_c could be obtained through the optimal couplings.

Further, we mention that optimal transport-based methods have been recently proposed in order to obtain fixed-size representations. First, the work in [16] proposes a framework that uses a mapping to obtain a linear approximation of the Wasserstein-2 distance. In order to obtain this mapping, the barycentric projection [17] from a reference to each graph representation is needed. The optimal transport plans, needed for the barycentric projection map calculation, are obtained by solving the Kantorovich problem [18] with linear solvers [19]. Once the graph representations of fixed size are obtained, they are used to perform various graph prediction tasks. As this framework is not differentiable, it cannot be integrated in end-to-end architectures for graph representation learning and only non-parametric graph representations are considered. Also, its performance relies heavily on the choice of the values of the representation of the reference, which must be numerically close to those of the graph representations. Second, in [20] the authors address the problem of finding fixed-size representations of sets of features of varying size and, possibly, in the regime where labeled data are scarce. They

introduce an embedding (OTKE) that combines kernel methods [21] and optimal transport. They propose to embed the feature representations of a set to a reproducing kernel Hilbert space and subsequently pool the obtained embedding using the optimal transport plan between the kernel embedding and a trainable reference. Furthermore, the relation of the proposed OTKE to attention mechanisms is discussed and its performance is validated on biological sequence classification and natural language processing tasks. Third, in [22] a Euclidean embedding using the generalized sliced Wasserstein distance [23] is proposed. It is shown that this embedding can be used to pool representations of sets of varying size in deep neural network architectures.

Finally, we would like to mention that more recently in [24] the authors propose Sinkformers², a variation of the transformer architecture [25] where the learnable attention matrices are forced to be doubly stochastic using Sinkhorn’s algorithm [26]. They consider the case where the attention blocks have tied weights between layers and show theoretically that, in the infinite depth limit, Sinkformers correspond to a Wasserstein gradient flow.

3 Preliminaries

3.1 The Optimal Transport Problem

Optimal Transport is a mathematical theory that allows to compare measures in a geometrically meaningful way. Given two discrete probability measures $\mu = \sum_{i=1}^n a_i \delta_{x_i}$ and $\nu = \sum_{j=1}^m b_j \delta_{y_j}$, the Kantorovich optimal transport problem [18] aims to find the optimal probabilistic coupling $P \in \mathbb{R}_+^{n \times m}$ between the measures μ and ν that minimizes the total cost of transportation:

$$\min_P \langle C, P \rangle \tag{1}$$

while satisfying the constraint:

$$P \in U(a, b) = \{P \in \mathbb{R}_+^{n \times m} | P \mathbf{1}_m = a \text{ and } P^\top \mathbf{1}_n = b\}. \tag{2}$$

The constraint in Eq. (2) guarantees that the entirety of the mass of measure μ , namely a , is transported to the mass of measure ν , namely b . The cost C in Eq. (1) is an $n \times m$ matrix that captures the geometry of the space on which the probability measures are defined, as captured by the pairwise relationships between the points in the support of the measures μ and ν .

The problem defined in Eq. (1), (2) is a linear program. Its feasible region is the convex polytope $U(a, b)$ defined by the mass preservation constraints. It can be solved using linear programming solvers such as the simplex algorithm [27].

From now on we will denote the Kantorovich optimal transport problem between the measures $\mu = \sum_{i=1}^n a_i \delta_{x_i}$, $\nu = \sum_{j=1}^m b_j \delta_{y_j}$ as $L_C(a, b)$. This is done in order to highlight the dependency of the problem both on the geometry and the distribution of mass. The geometry is dictated by the supports of the measures $\{x_i\}_{i=1}^n$, $\{y_j\}_{j=1}^m$ and the cost function $C(x, y)$ selected to penalize the transportation of mass from any x_i to any y_j . The distribution of mass is dictated by the weight vectors a and b . Therefore, from now on:

$$L_C(a, b) = \min_{P \in U(a, b)} \langle P, C \rangle. \tag{3}$$

In the specific case where the cost C is the p -th power of a metric D on the space Ω , it is shown through the Gluing Lemma (Theorem 7.3 in [2]) that $L_C(a, b)$ can be used to define the p -Wasserstein distance between the measures μ, ν as:

$$W_p(\mu, \nu) = L_{D^p}(a, b)^{\frac{1}{p}}. \tag{4}$$

Therefore, optimal transport offers a principled way to use the distance between the support of the measures to define a distance between the measures themselves.

²This work was published after the PhD defense and, therefore, this reference is not included in the respective thesis manuscript. However, we mention it in this pre-print article as interesting related work that studies the evolution of embeddings at the hidden layers of deep networks with respect to their Wasserstein distance.

3.2 Entropy Regularization

Since the Kantorovich problem defined in Eq. (3) is a linear program, the complexity of computing $L_C(a, b)$ scales in at least $\mathcal{O}((n + m)nm \log(n + m))$ when comparing discrete measures of n and m points. Also, the problem in Eq. (3) attains its minimum at a vertex of the feasible set $U(a, b)$. Therefore, the value $L_C(a, b)$ and the optimal coupling P^* are very susceptible to small changes in the measures μ and ν . Both of these issues of high computational complexity and instability to small perturbations are addressed by the entropic regularization of the optimal transport problem [28] proposed in the context of machine learning by Cuturi in 2013.

The entropy regularized optimal transport problem aims to find an optimal probabilistic coupling P between the measures μ and ν that minimizes the total cost of transportation and whose negative entropy is as small as specified by a regularization parameter ϵ . Given the entropy $H(P) = -\sum_{i=1}^n \sum_{j=1}^m P_{i,j} \log P_{i,j}$ of the coupling P , the regularized problem takes the form:

$$L_C^\epsilon(a, b) = \min_{P \in U(a, b)} \langle C, P \rangle - \epsilon H(P). \quad (5)$$

The problem in Eq. (5) can be solved with a fixed point algorithm, by alternating the updates:

$$u^{(l+1)} = \frac{a}{Kv^{(l)}} \text{ and } v^{(l+1)} = \frac{b}{K^\top u^{(l+1)}} \quad (6)$$

where the divisions are applied element-wise and the initialization is a positive vector, for instance $v^{(0)} = \mathbb{1}_m$. The iterations in Eq. (6) define Sinkhorn's matrix scaling algorithm [26] on the Gibbs kernel $K = e^{-\frac{C}{\epsilon}}$. Therefore, the solution of the entropy-regularized problem with Sinkhorn's algorithm consists of matrix-vector multiplications and element-wise divisions and its computational complexity is $\mathcal{O}((n + m)^2)$ when comparing measures of n and m points. The optimal coupling, as obtained after L Sinkhorn iterations is equal to:

$$P^* = \text{diag}(u^{(L)})K \text{diag}(v^{(L)}). \quad (7)$$

By considering dual variables f, g , we can obtain the dual formulation of the entropy-regularized transport problem as:

$$L_C^\epsilon(a, b) = \max_{f \in \mathbb{R}^n, g \in \mathbb{R}^m} \langle f, a \rangle + \langle g, b \rangle - \epsilon \langle e^{\frac{f}{\epsilon}}, K e^{\frac{g}{\epsilon}} \rangle. \quad (8)$$

The unconstrained maximization problem in Eq. (8) can be solved with block coordinate ascent [29]. The potentials f and g are updated alternatively by cancelling the respective gradients in these variables of the objective in Eq. (8).

4 Graph Representations as Probability Measures

In order to define a Wasserstein distance between graph representations, we first explain how we correspond the representation of a graph to a probability measure. Given a graph G of N nodes, its representation with d features is a $d \times N$ matrix $Y = [y_1, \dots, y_N]$ where y_j is the $d \times 1$ dimensional representation of the j -th node. We propose to describe the representation of the graph G as a probability measure:

$$\nu = \sum_{j=1}^N b_j \delta_{y_j}, \quad (9)$$

where $b \in \Sigma_N$ is a histogram. The value of b_j captures the significance of the representation of node j . In the case where all nodes are of equal importance we may consider $b_j = \frac{1}{N}, \forall j$. On the contrary, we can consider a non-uniform distribution on the nodes in order to account for some uncertainty in the node representation. For instance, in a social network, we may chose to use higher weights for nodes that correspond to users that have been members of the network for more that one year and whose features decrbe them well, and lower weights for users that have just joined the social network.

In Fig. (1) we provide an example. We consider a graph G of $N = 7$ nodes with representation $Y \in \mathbb{R}^{2 \times 7}$. The 2×1 dimensional feature representation of node j corresponds to $y_j = [Y_{1,j}; Y_{2,j}]$. We show on the left of Fig. (1) the graph G , where each node is annotated with its representation. We correspond to the representation of the graph G the probability measure $\nu = \sum_{j=1}^7 b_j \delta_{y_j}$. Assuming that all nodes have equal importance, the weights of the measure ν are equal to $b_j = \frac{1}{7}, \forall j$. The positions of mass of the probability measure ν are determined by the representations of the nodes y_j . On the right of Fig. (1) we plot the measure ν in the 2-dimensional Euclidean space.

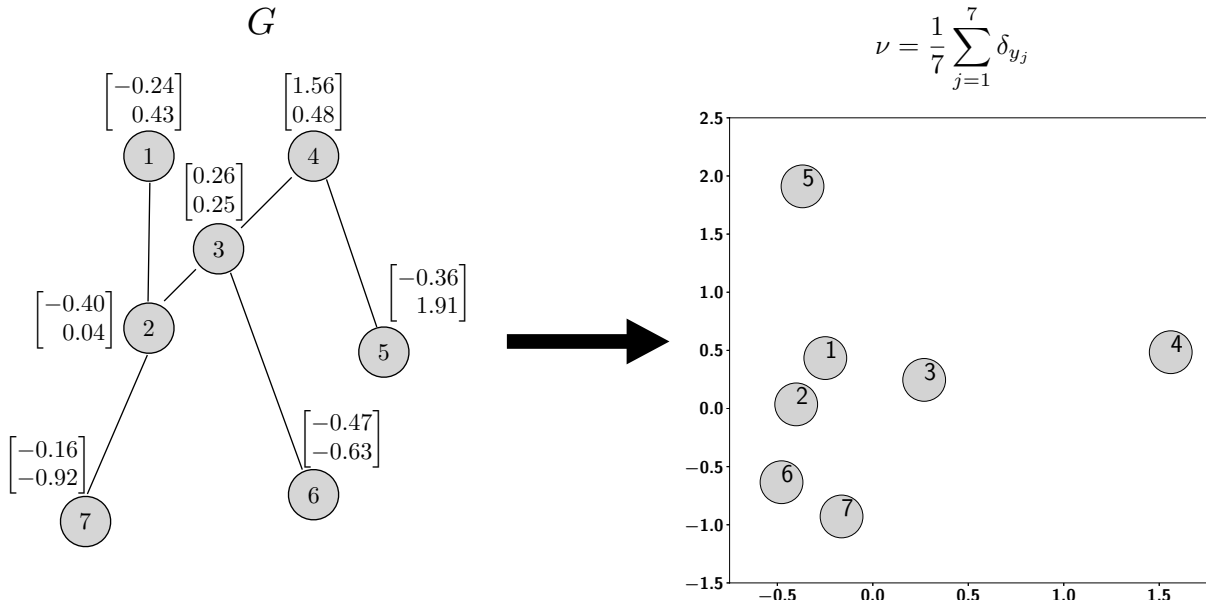


Figure 1: Corresponding a graph G to a probability measure ν . On the left we show a graph G of $N = 7$ nodes with its representation Y . The j -th node is annotated with its representation $y_j = [Y_{1,j}; Y_{2,j}]$. For instance, the representation of node 2 is $y_2 = [-0.40; 0.04]$. By assuming that all the nodes in graph G are equally important, we correspond the graph representation to the probability measure $\nu = \frac{1}{7} \sum_{j=1}^7 \delta_{y_j}$. The positions of mass of the measure are determined by the node representations.

5 FlowPool

The goal of global graph pooling is to transform a representation of a graph of N nodes in a d -dimensional feature space to a fixed size representation of M nodes with the same feature dimension d . Let $\nu = \sum_{j=1}^N b_j \delta_{y_j}$ and $\mu = \sum_{i=1}^M a_i \delta_{x_i}$ be the probability measures that correspond to the graph representation $Y \in \mathbb{R}^{d \times N}$ and its pooled counterpart $X \in \mathbb{R}^{d \times M}$. FlowPool computes the pooled representation X by solving:

$$\min_X L_{C(X,Y)}^\epsilon(a, b), \quad (10)$$

where $L_{C(X,Y)}^\epsilon(a, b)$ is the solution of the entropy regularized optimal transport problem defined in Eq.(5) for a cost $C = D^p$, with D a distance metric on the graph representation space $\Omega = \mathbb{R}^d$. We denote the cost of the mass transportation as $C(X, Y)$ in order to highlight the dependency of the cost C on X, Y . From now on, we assume that the nodes are of equal importance in all cases, so that $a = \frac{1}{M} \mathbb{1}_M$ and $b = \frac{1}{N} \mathbb{1}_N$.

The objective function in Eq. (10) is differentiable with respect to X . Therefore, we can compute the pooled graph representation by solving the problem in Eq. (10) with a gradient-based optimization method. Thus, our proposed pooling method is cast to a gradient flow. By denoting as $X^{(0)}$ the

initialization for the pooled graph representation and as $X^{(L)}$ the obtained pooled representation after L iterations of the gradient-based method that minimizes Eq. (10), FlowPool can be thought of as demonstrated in Fig. (2). Specifically, given an initialization $X^{(0)} \in \mathbb{R}^{d \times M}$, the FlowPool method summarizes any graph representation $Y \in \mathbb{R}^{d \times N}$, by performing L steps of a gradient-based method that minimizes the energy $L_{C(X,Y)}^\epsilon(a,b)$ ³. The returned pooled representation $X^{(L)}$ is the $d \times M$ representation that has minimal Wasserstein distance from the $d \times N$ input representation Y .

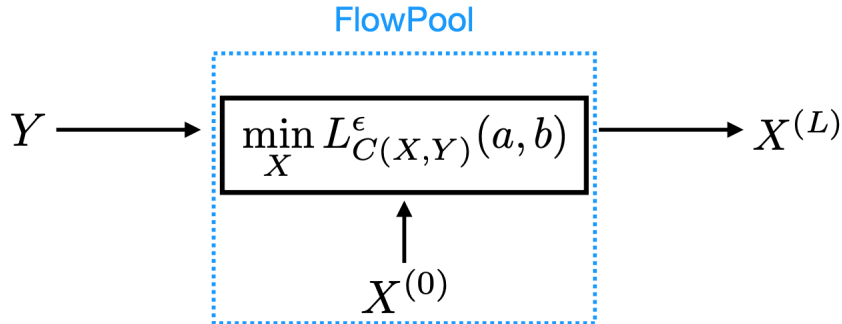


Figure 2: The FlowPool method for pooling graph representations. The input is a graph representation $Y \in \mathbb{R}^{d \times N}$, where N can admit any value. The output $X^{(L)}$ is a $\mathbb{R}^{d \times M}$ representation, with M fixed, such that $L_{C(X^{(L)},Y)}^\epsilon(a,b)$ is minimal.

6 Implementation of FlowPool

At each step of the gradient-based optimization of X , we need to compute the gradient with respect to X of the energy $L_{C(X,Y)}^\epsilon(a,b)$ for the current X . One possible way to compute this gradient is to back-propagate through the operations of the Sinkhorn iterations. A more efficient approach to compute $\nabla_X L_{C(X,Y)}^\epsilon(a,b)$ is by using the implicit function theorem [30]. The implicit differentiation of the entropy-regularized optimal transport problem is particularly more efficient in terms of memory requirements as not all intermediate calculations of the Sinkhorn iterations need to be stored in memory for the backpropagation.

6.0.1 Implicit Function Theorem

The implicit function theorem [30] states that, given a continuously differentiable function F , and a point $(x^*(\theta), \theta)$ such that $F(x^*(\theta), \theta) = 0$, if the Jacobian $\partial_1 F(x^*(\theta), \theta)$ is invertible, the variables $x(\theta)$ are differentiable functions of θ in some neighborhood of the point $(x^*(\theta), \theta)$. By applying the chain rule, we obtain:

$$\begin{aligned} \partial_1 F(x^*(\theta), \theta) \partial x^*(\theta) + \partial_2 F(x^*(\theta), \theta) &= 0 \Leftrightarrow \\ -\partial_1 F(x^*(\theta), \theta) \partial x^*(\theta) &= \partial_2 F(x^*(\theta), \theta), \end{aligned} \quad (11)$$

where by ∂_1, ∂_2 we denote the Jacobian with respect to the first and the second argument, accordingly. As a result, the Jacobian $\partial x^*(\theta)$ can be obtained by solving the linear system in Eq. (11).

The recent work in [1] proposes to use the implicit function theorem in order to perform automatic differentiation of optimization problems. In that context, θ stands for the inputs of the optimization problem, $x^*(\theta)$ for the optimal solution and the function F captures the optimality conditions. Thus, the implicit function theorem offers the possibility to obtain the Jacobian of the optimal solution with respect to the inputs of the optimization problem.

³We note that $L_{C(X,Y)}^\epsilon(a,b)$ corresponds to the p -th power of the entropy-regularized Wasserstein distance.

6.0.2 Implicit Differentiation of the Entropy Regularized Optimal Transport Problem

In this work we use the OTT toolbox [31], which offers an implementation of the implicit differentiation of the entropy-regularized optimal transport problem [32]. We outline briefly below its implementation and how we employ it to compute the gradient $\nabla_X L_{C(X,Y)}^\epsilon(a, b)$ in FlowPool.

By considering the dual formulation in Eq. (8), the computation of $L_{C(X,Y)}^\epsilon(a, b)$ consists in computing the optimal dual potentials f^*, g^* and the entropy regularized OT cost from these potentials using Eq. (8). Therefore, from the chain rule, we can obtain the gradient $\nabla_X L_{C(X,Y)}^\epsilon(a, b)$ as:

$$\nabla_X L_{C(X,Y)}^\epsilon(a, b) = \partial[f^*(X), g^*(X)]^\top \nabla_{[f^*(X), g^*(X)]} L_{C(X,Y)}^\epsilon(a, b), \quad (12)$$

where the gradient $\nabla_{[f^*(X), g^*(X)]} L_{C(X,Y)}^\epsilon(a, b)$ captures how changes in the optimal potentials $f^*(X), g^*(X)$ affect the entropy-regularized optimal transport cost and the transposed Jacobian $\partial[f^*(X), g^*(X)]^\top$ shows how changes in the positions X affect the optimal potentials $f^*(X)$ and $g^*(X)$.

The Jacobian $\partial[f^*(X), g^*(X)]$ can be computed using the implicit function theorem. As discussed in Section 3, the problem in Eq. (8) can be solved with block-coordinate ascent. As a result, the optimality conditions consist in cancelled gradients of the energy $\mathcal{E}(f, g) = \langle f, a \rangle + \langle g, b \rangle - \epsilon \langle e^{\frac{f}{\epsilon}}, K e^{\frac{g}{\epsilon}} \rangle$ with respect to f and g . Therefore, by considering the continuously differentiable function F as:

$$F([f(X), g(X)], X) = \begin{bmatrix} \nabla_f \mathcal{E}(f, g) \\ \nabla_g \mathcal{E}(f, g) \end{bmatrix}, \quad (13)$$

at optimality it holds that:

$$F([f^*(X), g^*(X)], X) = \begin{bmatrix} 0_M \\ 0_N \end{bmatrix}. \quad (14)$$

The implicit function theorem states that, provided that the Jacobian $\partial_1 F([f^*(X), g^*(X)], X)$ is invertible, we can obtain the Jacobian $\partial[f^*(X), g^*(X)]$ by solving a linear system, such as the one in Eq. (11). From Eq. (13), we can obtain $\partial_1 F([f(X), g(X)], X)$ as:

$$\partial_1 F([f(X), g(X)], X) = \begin{bmatrix} \partial_f \nabla_f \mathcal{E}(f, g) & \partial_g \nabla_f \mathcal{E}(f, g) \\ \partial_f \nabla_g \mathcal{E}(f, g) & \partial_g \nabla_g \mathcal{E}(f, g) \end{bmatrix}. \quad (15)$$

By evaluating the derivatives in Eq. (15) at the optimal potentials f^* and g^* it follows that:

$$-\partial_1 F([f^*(X), g^*(X)], X) = \frac{1}{\epsilon} \begin{bmatrix} \text{diag}(a) & P^* \\ P^{*\top} & \text{diag}(b) \end{bmatrix}, \quad (16)$$

where P^* is the optimal coupling obtained for the transportation problem and $\text{diag}(a), \text{diag}(b)$ are diagonal matrices, with elements in the diagonal corresponding to the marginals a and b , respectively.

The Jacobian $\partial_2 F([f^*(X), g^*(X)], X)$ can be computed with automatic differentiation. Due to the block structure of the Jacobian in Eq. (16), the linear system in Eq. (11) can be solved with Schur's complement [33]. The Schur complement that is inverted depends on which of the M or N is smaller. In either case, the Schur complement is rank deficient, with a 0 eigenvalue for the vector of ones. Therefore, a ridge kernel regularization is added that enforces solutions to have zero sum. Further, when two nodes in the graph representation Y have very similar feature representations, two columns of the cost C are numerically close and therefore two columns of the optimal coupling P^* are colinear. In order to deal with the rank deficiency of the Schur complement in that case, a ridge identity regularization is added. The linear system is solved with the conjugate gradient method [34]. Having solved the linear system with respect to $\partial[f^*(X), g^*(X)]$, and using the chain rule, we can obtain the desired gradient as in Eq. (12).

We show in Algorithm 1, the implementation of FlowPool for L iterations of the gradient flow. In line 3 we compute the optimal potentials f^*, g^* using block coordinate ascent, as described in Section 3. We use the implicit differentiation in line 5 to obtain the gradient as in Eq.(12) and update the pooled representation using this gradient in line 7. The geometry is captured by the cost function $C(X, Y)$,

which uses the input graph representation Y and its pooled counterpart $X^{(l)}$ at the l -th iteration, to return the cost matrix $C^{(l)}$. We denote with τ the step size used for the gradient flow.

Algorithm 1 FlowPool

Input: $Y; X^{(0)}$

- 1: **for** $l = 0$ to $L - 1$ **do**
 - 2: Solve Sinkhorn
 - 3: $f^*, g^* = \text{Sinkhorn}(a, b, C^{(l)} = C(X^{(l)}, Y), \epsilon)$
 - 4: Compute gradient with implicit function theorem
 - 5: $\nabla_X L_{C(X^{(l)}, Y)}^\epsilon(a, b) = \text{implicit_diff}(f^*, g^*, a, b, X^{(l)}, Y, \epsilon)$
 - 6: Update pooled graph representation:
 - 7: $X^{(l+1)} = \text{update_step}(X^{(l)}, \nabla_X L_{C(X^{(l)}, Y)}^\epsilon(a, b), \tau)$
 - 8: **end for**
 - 9: **return** $X^{(L)}$
-

7 Permutation Invariance

We now show that the proposed pooling method is permutation invariant. This is a particularly relevant property when performing global pooling of graph representations. If FlowPool is preceded by permutation equivariant message passing layers [35], the pooled graph representation is permutation invariant. This means that the predictions made for a given graph are independent of the ordering of its nodes.

7.1 Computation of $\nabla_X L_{C(X, Y)}^\epsilon(a, b)$

Although the gradient $\nabla_X L_{C(X, Y)}^\epsilon(a, b)$ is computed in an automatic way in FlowPool using implicit differentiation, as outlined in Section 6, we demonstrate now how it can be computed analytically in order to prove that FlowPool is invariant to permutations. For this derivation, we consider the primal formulation of the entropy-regularized problem which is equivalent to the dual formulation. In the primal formulation, the optimization variable is the coupling P , and the optimal coupling can be obtained from the optimal potentials f^*, g^* as:

$$P^* = e^{\frac{f^* \mathbf{1}_m^\top + \mathbf{1}_n g^{*\top} - C}{\epsilon}}. \quad (17)$$

Using the primal formulation, the gradient $\nabla_X L_{C(X, Y)}^\epsilon(a, b)$ can be expressed as:

$$\nabla_X L_{C(X, Y)}^\epsilon(a, b) = [\partial_X C(X, Y)]^\top \nabla_C L_{C(X, Y)}^\epsilon(a, b), \quad (18)$$

where $\nabla_C L_{C(X, Y)}^\epsilon(a, b)$ shows how changes in the cost matrix C affect the entropy-regularized cost $L_{C(X, Y)}^\epsilon(a, b)$ and the transposed Jacobian $[\partial_X C(X, Y)]^\top$ shows how changes in the positions X affect the cost matrix C . The computations in Eq. (12) and Eq. (18) are equivalent. In Eq. (18) however, the only term that depends on the solution of the optimal transport problem is $\nabla_C L_{C(X, Y)}^\epsilon(a, b)$. Therefore, it is more intuitive to study the differentiation with respect to X using the primal formulation.

By observing Eq. (5) one can notice that in the case of FlowPool the objective function that is being minimized is a function of two variables, the cost C and the coupling P . As a result, we can re-express Eq. (5) as:

$$L_C^\epsilon(a, b) = \min_{P \in U(a, b)} Q(C, P), \quad (19)$$

where:

$$Q(C, P) = \langle C, P \rangle - \epsilon H(P). \quad (20)$$

Therefore, the optimal coupling is obtained by:

$$P^*(C) = \underset{P \in U(a,b)}{\operatorname{argmin}} Q(C, P), \quad (21)$$

where we denote the coupling as $P^*(C)$ in order to highlight its dependency on the cost C . This dependency is a direct consequence of the Sinkhorn iterations in Eq. (6), the expression for the Gibbs kernel $K = e^{-\frac{C}{\epsilon}}$ and the factorization of the optimal coupling in Eq. (7).

From Eq. (19), (20), (21) we obtain that:

$$L_{C(X,Y)}^\epsilon(a, b) = Q(C, P^*(C)). \quad (22)$$

As a result, from the chain rule it follows that:

$$\nabla_C L_{C(X,Y)}^\epsilon(a, b) = \nabla_1 Q(C, P^*(C)) + [\partial_C P^*(C)]^\top \nabla_2 Q(C, P^*(C)), \quad (23)$$

where we denote by ∇_1 and ∇_2 the gradient with respect to the first and the second argument respectively.

Due to the envelope theorem [36], [37], we can approximate $Q(C, P^*(C))$ with a function $G(C) = Q(C, P^*)$, where P^* is assumed to be constant and independent of C . Therefore, we obtain:

$$\nabla_C L_{C(X,Y)}^\epsilon(a, b) = \nabla G(C) = P^*. \quad (24)$$

From Eq. (18), (24) it follows that:

$$\nabla_X L_C^\epsilon(a, b) = \left(\sum_{j=1}^N P_{i,j}^* \nabla_1 C(x_i, y_j) \right)_{i=1}^M. \quad (25)$$

7.2 Proof of Permutation Invariance

We consider a graph representation $Y_1 \in \mathbb{R}^{d \times N}$ and its column-wise, or equivalently node-wise, permutation according to an $N \times N$ permutation matrix \mathcal{P}_f :

$$Y_2 = Y_1 \mathcal{P}_f. \quad (26)$$

We will show that $\operatorname{FlowPool}(Y_1) = \operatorname{FlowPool}(Y_2)$.

7.2.1 OT cost

Let $X^{(0)} \in \mathbb{R}^{d \times M}$ be the initialization of the pooled graph representation and C_1, C_2 be the $M \times N$ cost matrices that capture the pairwise squared Euclidean distances from $X^{(0)}$ to Y_1 and to Y_2 , respectively. From Eq.(26) we obtain:

$$C_2 = C_1 \mathcal{P}_f. \quad (27)$$

7.2.2 OT coupling

Because of the entropic regularization, the problem in Eq. (5) is a strictly convex minimization problem. Given uniform weight distributions, $a = \frac{1}{M} \mathbb{1}_M$ and $b = \frac{1}{N} \mathbb{1}_N$, the only variable controlling the unique solution P^* is the cost for the transportation. Therefore, due to the relationship between the costs C_1, C_2 in Eq.(27), it holds that:

$$P_2^* = P_1^* \mathcal{P}_f. \quad (28)$$

7.2.3 Gradient

Due to Eq. (27), (28), and the expression for the gradient of $L_C^\epsilon(a, b)$ with respect to X in Eq. (25), it follows that the gradient $\nabla_X L_{C(X,Y)}^\epsilon(a, b)$ will be the same for both the permuted and the non-permuted case.

7.2.4 Update Step

As a result, if the initialization $X^{(0)}$ is common in both cases, then $X_1^{(1)} = X_2^{(1)}$. Similarly, we can show that this is true for all iterations $0 < l < L$ of the flow. Therefore, it holds that $X_1^{(L)} = X_2^{(L)} \Leftrightarrow \text{FlowPool}(Y_1) = \text{FlowPool}(Y_2)$. The assumption that $X^{(0)}$ is common for both cases is a reasonable one. In fact, as we demonstrate in Section 9, it is necessary for $X^{(0)}$ to be shared among all graph representations in order for our proposed pooling method to perform well. In Section 10, we discuss how one can go a step further by parametrizing $X^{(0)}$ and learning it from the data.

8 Integrating FlowPool in Graph Neural Network Architectures

In order to integrate FlowPool in end-to-end deep learning architectures for graphs an element that needs to be considered is the differentiation of the output of FlowPool with respect to its input. This differentiation is key in the general setting, where the input representation Y can be the output of one or more layers with trainable weights and we need to backpropagate through FlowPool in order to learn these weights. In order to backpropagate through FlowPool we need to compute the Jacobian of the output $X^{(L)}$ with respect to the input Y . In this section we outline how this computation is handled. We depict a block-scheme of the computations in FlowPool in Fig. (3).

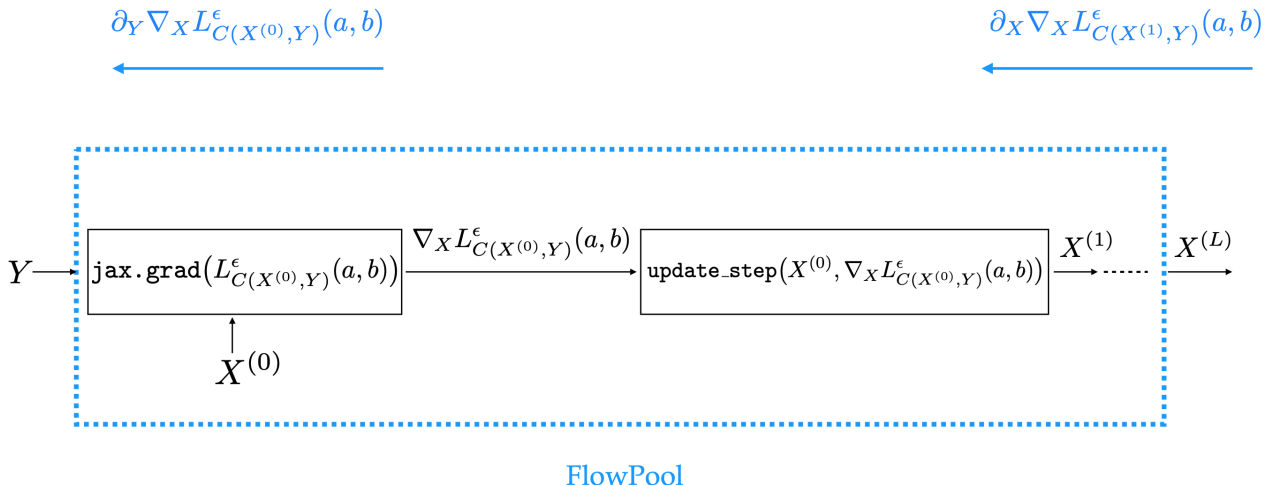


Figure 3: Implementation of FlowPool using JAX. The gradient $\nabla_X L_{C(X,Y)}^\epsilon(a, b)$ needed for the gradient flow is obtained with JAX’s function `jax.grad`. The pooled graph representation is updated according to this gradient. During the backpropagation the gradient function obtained with `jax.grad` is re-derived in order to obtain the Jacobians $\partial_Y \nabla_X L_{C(X,Y)}^\epsilon(a, b)$ and $\partial_X \nabla_X L_{C(X,Y)}^\epsilon(a, b)$.

The OTT toolbox used in this work is based on the automatic differentiation framework JAX [38]. In the forward pass of FlowPool the gradient $\nabla_X L_{C(X,Y)}^\epsilon(a, b)$, computed using the implicit differentiation scheme described above, is returned by calling JAX’s function `jax.grad` on the entropy regularized cost $L_{C(X,Y)}^\epsilon(a, b)$. In Fig. (3) we show how the pooled representation after the first step of the flow, $X^{(1)}$, is computed using the gradient $\nabla_X L_{C(X,Y)}^\epsilon(a, b)$ evaluated at $X^{(0)}$ and Y . At the backward pass, we need to differentiate again the function $\nabla_X L_{C(X,Y)}^\epsilon(a, b)$. We note that the envelope theorem does not hold for higher order derivatives and, therefore, the second term in Eq. (23) will be re-differentiated during the backpropagation. The re-derivation of the gradient function obtained with `jax.grad` is possible using JAX’s ability to perform automatic differentiation of the linear system in Eq. (11). Specifically, this is accomplished with JAX’s function `jax.lax.custom_linear_solve` that wraps all linear solvers in JAX [31] and allows to compute higher order derivatives, implicitly again.

At the backpropagation of the first step of the flow, the Jacobian needed is $\partial_Y \nabla_X L_{C(X^{(0)}, Y)}^\epsilon(a, b)$, which captures how the gradient $\nabla_X L_{C(X,Y)}^\epsilon(a, b)$ is affected by changes in the input graph representa-

tion Y , for the initialization of the pooled representation $X^{(0)}$. In the next steps of the flow, Jacobians of the form $\partial_X \nabla_X L_{C(X,Y)}^\epsilon(a, b)$ are also needed. We note that $\partial_X \nabla_X L_{C(X,Y)}^\epsilon(a, b) = \nabla_X^2 L_{C(X,Y)}^\epsilon(a, b)$, where ∇^2 stands for the Hessian matrix with second-order derivatives. The computation of the Jacobian of $X^{(1)}$ with respect to $\nabla_X L_{C(X^{(0)}, Y)}^\epsilon(a, b)$ is straightforward. For instance, in the case of a gradient update step of the form $X^{(1)} = X^{(0)} - \tau \nabla_X L_{C(X^{(0)}, Y)}^\epsilon(a, b)$, it will be equal to $-\tau I$. Therefore, using JAX’s automatic differentiation we can compute the Jacobian of $X^{(L)}$ with respect to Y , and therefore backpropagate through FlowPool in order to train the layers that provide the graph representation Y .

9 Experiments

9.1 Experimental Analysis

In this Section we analyse the behaviour of FlowPool and the dependence on its parameters. For this analysis we consider the simplified setting where FlowPool is not integrated in a deep network. Further, we use the squared Euclidean distance cost in order to visualize the representations and build intuitions with regards to the way that FlowPool operates.

9.1.1 Experimental Settings

We consider two chemical compound datasets BZR and COX2 [39]. The chemical compounds are represented by graphs, where nodes correspond to atoms and edges represent chemical bonds. Each node is described by a 3-dimensional feature vector. The chemical compounds considered are benzodiazepine receptor ligands in BZR and cyclooxygenase-2 inhibitors in COX2. Further, the graphs are labeled as active or inactive against some type of cell. Therefore, the datasets can be used for binary graph classification. We provide the statistics of the datasets in Table 1.

Table 1: Statistics of Datasets

Dataset	# graphs	# classes	avg. node #	avg. edge #	# node features
BZR	405	2	35.75	38.36	3
COX2	467	2	41.22	43.45	3

In our experimental analysis, the representation Y of a graph corresponds to the features of its nodes, as provided by the dataset. As a result, a graph of N nodes corresponds to a representation $Y \in \mathbb{R}^{3 \times N}$.

The setup considered for our analysis is shown in Fig. (4). We consider the input to FlowPool to be a graph representation Y . FlowPool is used to pool Y to the fixed-size representation $X^{(L)}$, which

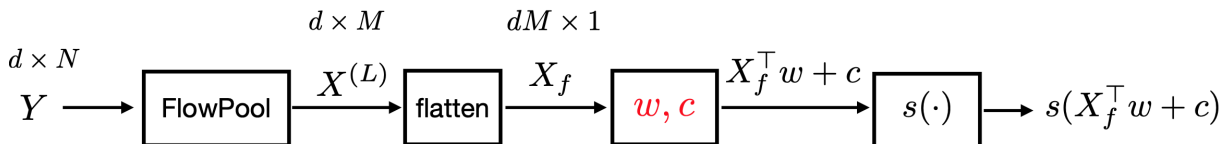


Figure 4: Block scheme of graph classification with FlowPool. FlowPool is used to pool a provided graph representation Y to a graph representation of fixed size $X^{(L)}$. The representation $X^{(L)}$ is flattened to obtain the representation X_f . The learnable parameters are the weights w and the intercept c of the logistic regression classifier, which are annotated with red. The features in X_f are linearly combined and passed through the sigmoid function, in order to obtain the probability that the graph representation Y belongs to the positive class.

is input to a logistic regression classifier. We train the classifier by minimizing the cross-entropy loss with an l_2 regularization on the weights, in order to avoid over-fitting. The weights w and intercept c of the classifier are the only learnable parameters. We denote the sigmoid function as:

$$s(\theta) = \frac{e^\theta}{e^\theta + 1}. \quad (29)$$

The considered datasets are not split into pre-defined training and test sets. Therefore, we evaluate the classification task over 10 different partitions of the data using 10 folds, as in a 10-fold cross validation scheme. For each partition, we use the 9 folds as our training data and the remaining fold for evaluation, and provide the mean and standard deviation of the classification accuracy for the 10 partitions. Further, we notice that the datasets BZR and COX2 are characterized by a class imbalance, as shown in Table 2. This is a common issue in biological datasets, such as the ones considered here. In order to properly take into account this imbalance, we consider stratified splits and we compute the balanced classification accuracy [40]. In the binary case, the balanced accuracy is equal to the arithmetic mean of sensitivity (true positive rate) and specificity (true negative rate):

$$\text{balanced accuracy} = \frac{1}{2} \left(\frac{TP}{TP + FN} + \frac{TN}{TN + FP} \right), \quad (30)$$

where TP, FP, TN, FN stand for true positives, false positives, true negatives and false negatives, respectively.

In what follows, we study the impact of the entropy regularization parameter and the removal of the bias of the entropic regularization. Further, we discuss the effect of the initialization of the pooled graph representations. Finally, we evaluate the performance of FlowPool on a binary classification task by comparing to other graph pooling methods.

Table 2: Class Imbalance

Dataset	% positive class	% negative class
BZR	21.23	78.77
COX2	21.84	78.16

9.1.2 Impact of Entropy Regularization

First, we study the impact of the entropy regularization parameter on the pooled graph representation. In order to do so, we consider values of the regularization parameter in $\epsilon = [0.01, 0.1, 1, 10, 100]$. Using the classification set-up of Fig. (4), with the same stratified splits for all the evaluations and for $M = 10$, we compute the mean and the standard deviation of the balanced classification accuracies over the 10 partitions of the data. We set the number of iterations of the gradient flow to $L = 200$ and the step size to $\tau = 0.2$. The results are shown in Fig. (5a) and Fig. (6a) for the BZR and COX2 datasets respectively. It can be seen that the value of ϵ affects the classification accuracy obtained. Further, we notice that for $\epsilon = 100$ there is a significant drop in the performance for both datasets. In order to explain why this is the case, we demonstrate in Fig. (7), (8) the representations obtained with FlowPool for different values of ϵ for the BZR and COX2 datasets, respectively. We show with blue the initial representation Y input to FlowPool and with red its pooled counterpart after L iterations of the flow. It can be seen that, as the values of the entropic regularization become larger, the pooled embeddings tend to “collapse”. In the extreme case of $\epsilon = 100$, the pooled representation yields the mean value of Y , since we use the squared Euclidean distance cost, and our method becomes equivalent to mean pooling. Further, we notice that for COX2 there is a clear trend of a dampening in its performance for larger values of ϵ , while for BZR there is a small increase for $\epsilon = 10$. We believe that this indicates that a smaller pooling dimension M may be the optimal for this dataset.

Interestingly the impact of the parameter ϵ has a very intuitive interpretation. We remind that:

$$L_C^\epsilon(a, b) = \min_{P \in U(a, b)} \langle C, P \rangle - \epsilon H(P). \quad (31)$$

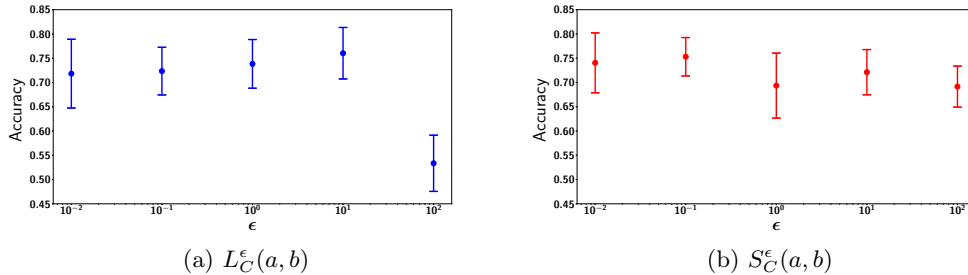


Figure 5: Impact of the entropy regularization parameter ϵ on the classification accuracy for the BZR dataset using FlowPool for the minimization of (a) the entropy regularized Wasserstein distance $L_C^\epsilon(a, b)$ and (b) the Sinkhorn divergence $S_C^\epsilon(a, b)$.

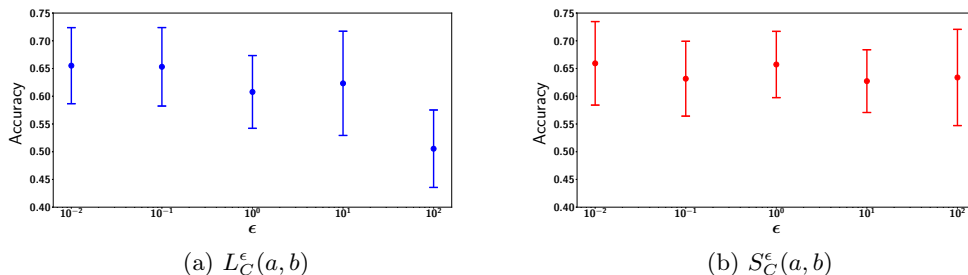


Figure 6: Impact of the entropy regularization parameter ϵ on the classification accuracy for the COX2 dataset using FlowPool for the minimization of (a) the entropy regularized Wasserstein distance $L_C^\epsilon(a, b)$ and (b) the Sinkhorn divergence $S_C^\epsilon(a, b)$.

Equivalently, as discussed in [41], we can write:

$$L_C^\epsilon(a, b) = \min_{P \in U(a, b)} \langle C, P \rangle + \epsilon \text{KL}(P|ab^\top). \quad (32)$$

We can observe that the quantity $\text{KL}(P|ab^\top)$ is equal to the mutual information of the probability measures ν and μ that correspond to the input graph representation and its pooled counterpart respectively (Section 4). The mutual information is minimal, and equal to zero, when the measures μ, ν are independent and the probabilistic coupling corresponds to the independence matrix $P = ab^\top$. As can be seen from Eq. (31), the optimal coupling will correspond to ab^\top when $\epsilon \rightarrow \infty$. As a result, in order to maximize the mutual information between μ and ν , while enjoying the properties of well defined gradients provided by the entropic regularization, one should chose small values for ϵ .

The collapse of the pooled graph representation, as demonstrated in Fig. (7), (8), is due to what is commonly referred to as the entropic bias. The entropy-regularized optimal transport loss between a measure $\nu = \sum_{j=1}^N b_j \delta_{y_j}$ and itself is equal to $L_{C(Y, Y)}^\epsilon(b, b)$, where $C(Y, Y)$ denotes the $N \times N$ cost matrix with the pairwise distances between the points $\{y_j\}_{j=1}^N$. For $\epsilon > 0$, $L_{C(Y, Y)}^\epsilon(b, b) \neq 0$ and, as a result, the minimization of $L_{C(X, Y)}^\epsilon(a, b)$ with respect to the positions of the measure μ leads to a biased solution, with the measure μ having a smaller support than that of the target measure ν . In [41], it is shown that a principled way to remedy that is to minimize instead the Sinkhorn divergence:

$$S_{C(X, Y)}^\epsilon(a, b) = L_{C(X, Y)}^\epsilon(a, b) - \frac{1}{2} L_{C(X, X)}^\epsilon(a, a) - \frac{1}{2} L_{C(Y, Y)}^\epsilon(b, b). \quad (33)$$

We consider again the experiment described above for values of the regularization parameter in $\epsilon = [0.01, 0.1, 1, 10, 100]$, while substituting the computation of $L_{C(X, Y)}^\epsilon(a, b)$ with the Sinkhorn divergence $S_{C(X, Y)}^\epsilon(a, b)$. The values of τ and L are kept the same. We show in Fig. (5b), (6b) the classification accuracies obtained for the BZR and COX2 datasets, respectively. It can be seen that, since the entropic bias has been removed, the impact of the value of ϵ on the classification accuracy is practically

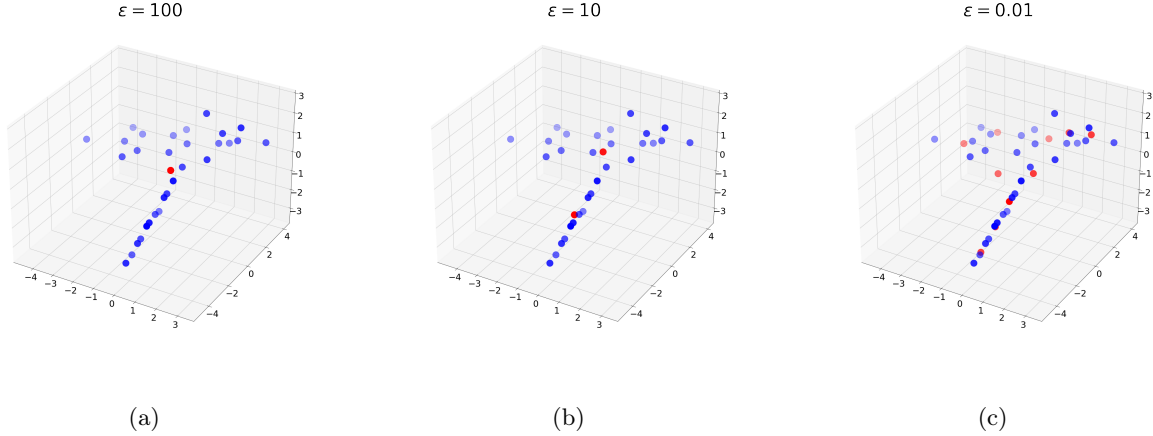


Figure 7: Pooled graph representations for different values of ϵ for a representation from BZR. With blue we show the initial representation $Y \in \mathbb{R}^{3 \times 30}$ and with red the pooled graph representation $X^{(L)} \in \mathbb{R}^{3 \times 10}$. Larger values of ϵ result to degenerate pooled representations $X^{(L)}$ with smaller support than Y .

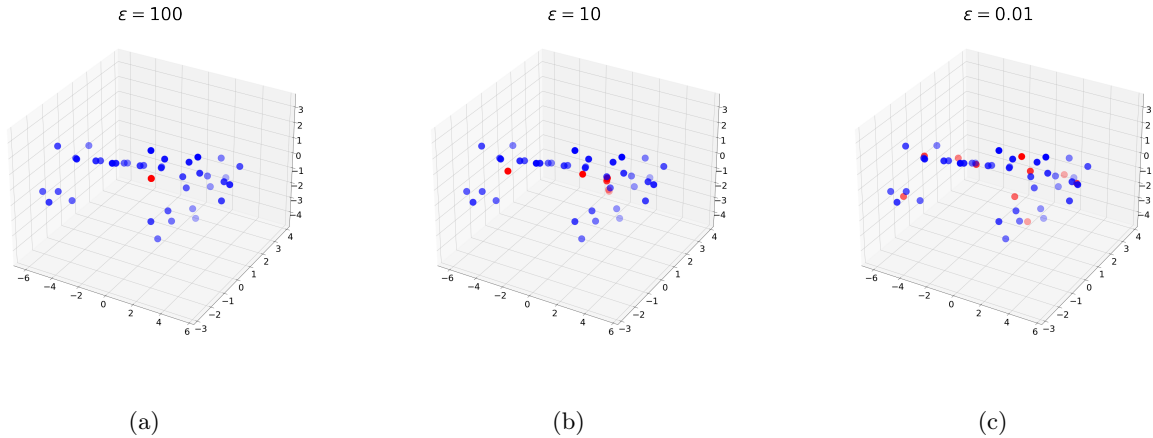


Figure 8: Pooled graph representations for different values of ϵ for a representation from COX2. With blue we show the initial representation $Y \in \mathbb{R}^{3 \times 39}$ and with red the pooled graph representation $X^{(L)} \in \mathbb{R}^{3 \times 10}$. Larger values of ϵ result to degenerate pooled representations $X^{(L)}$ with smaller support than Y .

eliminated. We show in Fig. (9), (10), examples of the representations obtained when the energy minimized is that of the entropy regularized Wasserstein distance and that of the Sinkhorn divergence. It can be seen that for the case of the Sinkhorn divergence, the pooled representation is not degenerate, even for the large value of $\epsilon = 10$. Therefore, the minimization of the Sinkhorn divergence constitutes FlowPool less sensitive to the hyperparameter ϵ and improves the quality of the pooled representation. Further, the Sinkhorn divergence offers an advantage in terms of computational complexity. This is due to the fact that larger values of ϵ can be considered without the “collapse” of the pooled embedding. As less iterations are needed for Sinkhorn to converge with larger values of ϵ , it follows that the Sinkhorn divergence is computationally more advantageous. As discussed in [41], the autocorrelation terms in Eq. (33) converge in a very small number of iterations and, therefore, their computational overhead is negligible. We note that in the case of FlowPool, only the autocorrelation term $L_{C(X,X)}^\epsilon(a, a)$ provides non-zero gradients with respect to X .

To sum up, the Sinkhorn divergence should be preferred over the entropy-regularized Wasserstein distance since it constitutes FlowPool less sensitive to the hyperparameter ϵ and less computationally

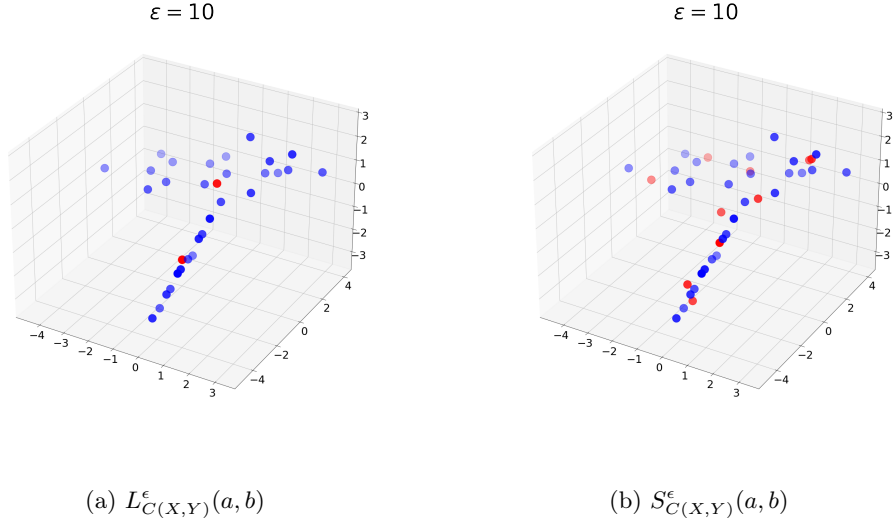


Figure 9: Comparison of the result of FlowPool on the feature representation of a graph from the BZR dataset for (a) the entropy regularized Wasserstein distance $L_{C(X,Y)}^\epsilon(a, b)$ and (b) the Sinkhorn divergence $S_{C(X,Y)}^\epsilon(a, b)$ for $\epsilon = 10, \tau = 0.2, L = 200$. It can be seen that the Sinkhorn divergence yields an unbiased solution even for this large value of $\epsilon = 10$.

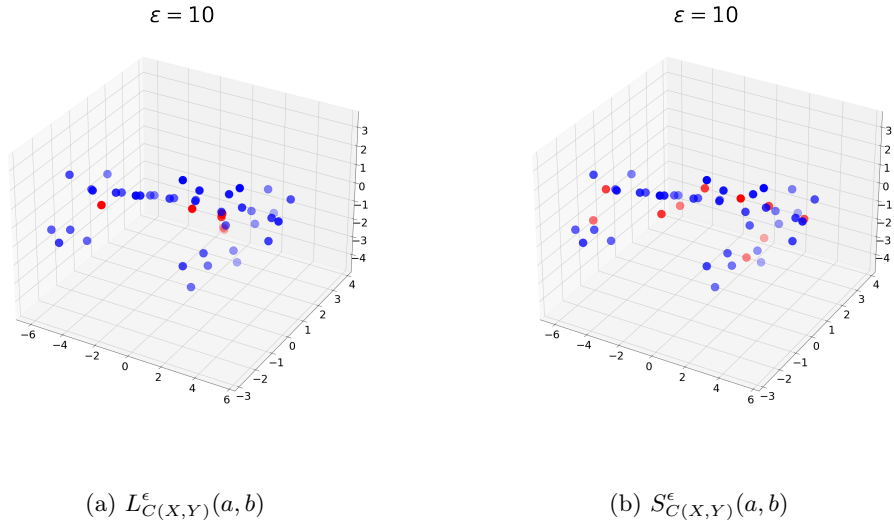


Figure 10: Comparison of the result of FlowPool on the feature representation of a graph from the COX2 dataset for (a) the entropy regularized Wasserstein distance $L_{C(X,Y)}^\epsilon(a, b)$ and (b) the Sinkhorn divergence $S_{C(X,Y)}^\epsilon(a, b)$ for $\epsilon = 10, \tau = 0.2, L = 200$. It can be seen that the Sinkhorn divergence yields an unbiased solution even for this large value of $\epsilon = 10$.

expensive. The optimal values of ϵ and M can be cross-validated based on the data under consideration and the task at hand.

9.1.3 Initialization of the Pooled Representation

The initialization $X^{(0)}$ impacts directly the pooled representation output by FlowPool. This is due to the fact that the optimization problem in Eq. (10) is non-convex with respect to X . Further, we notice that in order for FlowPool to yield meaningful representations, the initialization $X^{(0)}$ must be shared among all input graph representations Y . In order to demonstrate this, we consider the experimental setting of Section 9.1.1 with $M = 10$. We set $\tau = 0.2, L = 200, \epsilon = 0.1$ and use

the Sinkhorn divergence. We compute the classification accuracy for BZR and COX2 for the case where the initialization is fixed, and shared among all representations, and for the case where the initialization varies and is different for each input representation. The obtained accuracies using the same stratified folds are shown in Table 3. Three different initialization seeds are used in order to smooth the effect of unfavorable random initialization. It can be seen that the accuracies obtained when the initialization is shared among all inputs are significantly higher than the ones obtained for the case where the initialization is different for each input.

Table 3: Impact of Fixed Initialization.

Dataset	FlowPool (f. i.)	FlowPool
BZR	72.51 \pm 5.57	54.82 \pm 6.49
COX2	63.24 \pm 5.18	50.96 \pm 7.24

The reason why this is the case is the following. Let us consider a representation Y_1 , with pairwise distances from $X^{(0)}$, captured by the cost C_1 . If a representation Y_2 , that is close to Y_1 , is considered, the cost matrix C_2 will have similar values to those of C_1 . As a result, the optimal coupling P_1^* will be close to P_2^* . Given the same initialization $X^{(0)}$, due to Eq. (25), the gradient $\nabla_X L_{C(X,Y)}^\epsilon(a,b)$ evaluated at $(X^{(0)}, Y_1)$ will have similar values to that evaluated at $(X^{(0)}, Y_2)$ and consequently the pooled representations $X_1^{(1)}$ and $X_2^{(1)}$ will also be close. We can reason in a similar way for the next steps of the flow. Therefore, by using the same initialization for the source of the two transportation problems, we manage to obtain a sense of the similarity of the input representations Y_1, Y_2 .

9.1.4 Graph Classification

Having analysed the impact of the parameters of FlowPool on its performance, we now evaluate its efficiency in pooling graph representations compared to other methods. In order to evaluate the effectiveness of FlowPool, we consider the classification set-up of Fig. (4) and compare to other methods by substituting the FlowPool block with the following node clustering methods:

- K-means++ clustering [42]: The K-Means algorithm clusters the N node representations in $Y \in \mathbb{R}^{d \times N}$ by separating them into groups of equal variance. The centroids are initialized with the K-means++ initialization [43].
- K-means clustering with fixed random initialization: The K-means algorithm, where the centroids of the clusters are initialized randomly, but are shared across all input representations.
- Spectral Clustering (SC)[44]: SC performs a low-dimensional embedding of the Laplacian matrix of a graph, followed by clustering of the components of the eigenvectors in the low dimensional space.
- DiffPool [8]: DiffPool learns assignment matrices from the data by parametrizing them as $S = \text{softmax}(\text{GCN}(A, F))$, where A and F correspond to the adjacency matrix and the features of a graph, respectively. GCN corresponds to the graph convolutional filter [45] defined as $\text{GCN}(A, F) = \tilde{D}^{-\frac{1}{2}} \tilde{A} \tilde{D}^{-\frac{1}{2}} F \Theta$, where $\Theta \in \mathbb{R}^{d \times M}$ are the trainable weights, $\tilde{A} = A + I_N$ and \tilde{D} is the diagonal matrix of node degrees of \tilde{A} .
- MinCutPool [13]: MinCutPool parametrizes the assignment matrices as $S = \text{softmax}(F \Theta)$, where $\Theta \in \mathbb{R}^{d \times M}$ are the weights that are learned from the data. A regularizer, which approximates the relaxed formulation of the minCUT problem, affects the learned values of the trainable parameters Θ .

In the set-up we consider, we do not learn $X^{(0)}$, but initialize it randomly. Therefore, in order to compare to node clustering pooling methods, we consider fixed and random weights for their parameters as well. In order to mitigate the effect of possible favourable or unfavourable initializations on test performances, we consider three different random seeds for the initialization. For K-means++ the

random initialization will affect the selection of the cluster centers from the datapoints. In the case of K-means with fixed random initialization, the seeds will affect the initialization of the centroids that is shared among all input representations. In the case of Spectral Clustering, the random initialization pertains to the initialization of the clusters in the low-dimensional space. For DiffPool, MinCutPool and FlowPool the random initialization affects the parameters of the GCN layer, the fully connected layer and the initialization of the source $X^{(0)}$, respectively. For FlowPool we set $\tau = 0.2$, $L = 200$, $\epsilon = 0.1$ and use the Sinkhorn divergence. All methods are compared over the same stratified splits and the same random seeds. The classification accuracies are averaged over the ten partitions and the three different random initializations. The mean and the standard deviation of the obtained accuracies for all methods are shown in Table (4). It can be seen that, for both datasets, FlowPool yields the highest classification accuracy. For the BZR dataset, DiffPool and MinCutPool achieve the second best performance and their accuracies are comparable. We notice that Spectral Clustering does not perform well in pooling the node representations for the BZR dataset. For the COX2 dataset, the second best performance is achieved by K-means with fixed initialization, followed by SC. The reason why K-means with fixed initialization performs relatively well for both datasets is due to the fact that there is a close relationship between K-means and the minimization of the unregularized Wasserstein distance (as in Eq. (4)). This relationship is studied in [46], [47]. Finally, we observe that K-means++ performs poorly for both datasets. The reason for this stems from the fact that the K-means++ initialization is an algorithm that selects in a systematic way K points of the data as the centroids for the clustering. Therefore, the initialization for K-means in that case is not common for all input representations and, as a result, performance is hindered.

Table 4: Graph Classification Accuracy.

Dataset	K-means++	K-means (f.i.)	SC	DiffPool	MinCutPool	FlowPool
BZR	50.80 \pm 6.97	68.87 \pm 7.41	59.24 \pm 7.98	71.04 \pm 4.85	70.64 \pm 5.05	72.51 \pm 5.57
COX2	54.09 \pm 8.38	62.73 \pm 7.62	61.09 \pm 7.84	60.77 \pm 8.59	60.56 \pm 8.14	63.24 \pm 5.18

In the comparison carried out here, the only methods that use the graph structure are SC and DiffPool. MinCutPool, in the scenario of random weights considered, does not use structural information. This is because the minCUT regularizer can only impact the parameters Θ during training. FlowPool also does not take into account the graph structure as the cost C considered here employs only the similarity of the features, as captured by the squared Euclidean distance.

9.2 Preliminary Classification Results of FlowPool in a GNN

We now use FlowPool in order to perform global pooling in a GNN architecture. For this experiment we use the PROTEINS [48], [49] dataset. Proteins are represented as graphs, where nodes correspond to secondary structure elements (helix, sheet, turn) and two nodes are connected by an edge if they are neighbors along the amino-acid sequence or one of three nearest neighbors in space. The dataset consists of 1113 graphs with average node number $\bar{N} = 39.06$ and average edge number $\bar{E} = 72.82$. Further, each node is labeled according to its type using a one-hot encoded vector. We perform a binary classification task where we predict whether proteins are enzymes or not.

In order to do so, we consider a GNN composed of a graph convolutional layer [45], a global pooling layer and a fully connected layer followed by a sigmoid activation. The network is trained by minimizing the binary cross-entropy loss⁴. We use the same assessment method with 10-fold CV and the same stratified splits as those proposed in the paper for fair comparison of GNNs in the task of graph classification [53]. With this experiment we are solely interested in assessing the possibility of the integration of FlowPool in end-to-end deep learning architectures. Therefore, no model selection is performed in order to optimally tune hyperparameters. We keep the GNN architecture fixed and compare the classification accuracy obtained when using as the global pooling layer DiffPool, MinCutPool and FlowPool with random weights. All models are trained with Adam [54] with a learning

⁴Software: For the implementation of the GCN layer we use J-Raph [50]. For the gradient processing and optimization we use Optax [51]. The neural network library used is Haiku [52].

rate of $\mu = 0.0001$ and batch size = 8. The embedding dimension is set to $d = 3$ in order for us to visualize the representations and ensure that our method functions as expected when integrated in a GNN. The size of the pooled representation is set to $M = 20$. For FlowPool we set $\epsilon = 0.2$, $\tau = 0.1$ and $L = 2000$ and use the Sinkhorn divergence in order to remove the entropic bias. The pooled graph’s representation $X^{(0)}$ is set by randomly selecting M samples from the normal distribution $\mathcal{N}(0_d, I_d)$. We train over 1000 epochs and perform early-stopping [55] with a patience of 50 epochs in order to avoid overfitting. The criterion for early-stopping is based on the validation loss. We report the mean and the standard deviation of the classification accuracy over the 10 folds in Table 5. It can be seen that our proposed pooling method performs on par with MinCutPool and offers a small advantage in performance compared to DiffPool. We note that the performance of all methods can be improved by optimally selecting their hyperparameters. We expect that with optimal tuning, FlowPool will perform significantly better than other methods, as in Section 9.1.4. With this preliminary experiment, we have, however, performed a sanity check of the possibility of integrating FlowPool in end-to-end deep learning architectures for graphs.

Table 5: Classification Accuracy for PROTEINS.

Dataset	DiffPool	MinCutPool	FlowPool
PROTEINS	69.27 \pm 5.77	71.26 \pm 3.87	71.45 \pm 4.22

We highlight that the performance of a GNN network with FlowPool depends on the solution $\partial[f^*(X), g^*(X)]$ of the linear system that occurs during the implicit differentiation. In the forward pass, the solution of this linear system provides the gradient $\nabla_X L_{C(X,Y)}^\epsilon(a, b)$ via Eq. (12). In the backward pass, it affects the propagation of the derivatives through the Jacobians $\partial_Y \nabla_X L_{C(X,Y)}^\epsilon(a, b)$, $\partial_X \nabla_X L_{C(X,Y)}^\epsilon(a, b)$, which also depend on $\partial[f^*(X), g^*(X)]$ through Eq. (12). Therefore, in order to guarantee that both the forward and the backward pass behave as expected, we must ensure that the possible rank deficiency of the matrix in Eq. (16) is properly accounted for by selecting appropriate values for the regularizers that enforce the stability of the linear system. Finally, we note that during the backward pass and, therefore, the differentiation of $\nabla_X L_{C(X,Y)}^\epsilon(a, b)$, the second term in Eq. (23) affects the Jacobians $\partial_Y \nabla_X L_{C(X,Y)}^\epsilon(a, b)$, $\partial_X \nabla_X L_{C(X,Y)}^\epsilon(a, b)$.

By working on the numerical issues discussed, we expect the performance of FlowPool when integrated in GNNs to become significantly better than that of competing methods. Finally, we underline that the squared Euclidean distance was used as a cost matrix in these experiments mostly in order to provide intuitive visualizations and comprehension of the way that FlowPool operates. The investigation of different costs is possible due to the automatic differentiation framework discussed in Sections 6, 8.

10 Parametrization of FlowPool - Learning the Ground Cost

The pooled representations returned by FlowPool can become more relevant to the specific dataset, used to train the GNN architecture, by considering a parametrization of the ground cost $C = C(X, Y)$ used for the mass transportation. Two types of parametrization are possible. The first is to consider a known cost function $C(X, Y)$, such as the squared Euclidean cost used in the previous section, and learn the initialization $X^{(0)} \in \mathbb{R}^{d \times M}$ from the data. The second option is to consider a parametrization of the function $C(X, Y)$ in order to take into account the structures of the considered graphs. This corresponds to the problem of ground metric learning and has been studied in a line of works, such as [56], [57], [58], [59], among others. We believe that learning an appropriate cost from the data could offer a promising direction for future work. Our implementation of FlowPool with automatic differentiation ensures that the relevant derivatives can be computed for any cost C that captures the pairwise relationship between the input representation and its pooled counterpart.

11 Conclusion

In this work we proposed FlowPool, a framework for pooling graph representations, while optimally preserving their statistical properties. Our proposed method is framed as a Wasserstein gradient flow in the graph representation space and admits an intuitive parametrization. We proposed a versatile implementation of our method, based on automatic differentiation, that can take into account the geometry of the representation space through any optimal transport cost. We performed an experimental analysis of FlowPool on simplified settings and showed promising results on graph classification. Finally, we demonstrated that our method can be integrated in end-to-end deep learning architectures for graphs and provided directions for future work.

Acknowledgements

The author would like to thank: Pascal Frossard for supporting this work and for providing comments; Marco Cuturi for his kind interaction through the Github issues of the OTT toolbox, for the modifications in the source code that enabled the computation of second-order derivatives and for the clarifying comments regarding the envelope theorem and the derivation of the gradient of the entropy-regularized Wasserstein distance; Dorina Thanou and Thibault Séjourné for providing feedbacks.

References

- [1] M. Blondel, Q. Berthet, M. Cuturi, R. Frostig, S. Hoyer, F. Llinares-López, F. Pedregosa, and J.-P. Vert, “Efficient and modular implicit differentiation,” *arXiv e-prints*, pp. arXiv–2105, 2021.
- [2] C. Villani, *Optimal transport: old and new*. Springer Science & Business Media, 2008, vol. 338.
- [3] G. Peyré, M. Cuturi *et al.*, “Computational optimal transport,” Tech. Rep., 2017.
- [4] M. Zhang, Z. Cui, M. Neumann, and Y. Chen, “An end-to-end deep learning architecture for graph classification,” in *Proceedings of the AAAI Conference on Artificial Intelligence*, vol. 32, no. 1, 2018.
- [5] N. Shervashidze, P. Schweitzer, E. J. Van Leeuwen, K. Mehlhorn, and K. M. Borgwardt, “Weisfeiler-lehman graph kernels.” *Journal of Machine Learning Research*, vol. 12, no. 9, 2011.
- [6] H. Gao and S. Ji, “Graph u-nets,” in *Proceedings of the 36th International Conference on Machine Learning (ICML)*. PMLR, 2019, pp. 2083–2092.
- [7] J. Lee, I. Lee, and J. Kang, “Self-attention graph pooling,” in *Proceedings of the 36th International Conference on Machine Learning (ICML)*. PMLR, 2019, pp. 3734–3743.
- [8] Z. Ying, J. You, C. Morris, X. Ren, W. L. Hamilton, and J. Leskovec, “Hierarchical graph representation learning with differentiable pooling,” in *Advances in Neural Information Processing Systems (NeurIPS)*, 2018.
- [9] H. Yuan and S. Ji, “Structpool: Structured graph pooling via conditional random fields,” in *International Conference on Learning Representations (ICLR)*, 2020.
- [10] Y. G. Wang, M. Li, Z. Ma, G. Montúfar, X. Zhuang, and Y. Fan, “Haar graph pooling,” in *Proceedings of the 37th International Conference on Machine Learning (ICML)*.
- [11] A. Haar, “Zur theorie der orthogonalen funktionensysteme,” *Mathematische Annalen*, vol. 69, no. 3, pp. 331–371, 1910.
- [12] D. K. Hammond, P. Vandergheynst, and R. Gribonval, “Wavelets on graphs via spectral graph theory,” *Applied and Computational Harmonic Analysis*, vol. 30, no. 2, pp. 129–150, 2011.

- [13] F. M. Bianchi, D. Grattarola, and C. Alippi, “Spectral clustering with graph neural networks for graph pooling,” in *Proceedings of the 37th International Conference on Machine Learning (ICML)*. ACM, 2020, pp. 2729–2738.
- [14] G. Dantzig and D. R. Fulkerson, “On the max flow min cut theorem of networks,” *Linear inequalities and related systems*, vol. 38, pp. 225–231, 2003.
- [15] D. Mesquita, A. Souza, and S. Kaski, “Rethinking pooling in graph neural networks,” *Advances in Neural Information Processing Systems (NeurIPS)*, vol. 33, 2020.
- [16] S. Kolouri, N. Naderializadeh, G. K. Rohde, and H. Hoffmann, “Wasserstein embedding for graph learning,” in *International Conference on Learning Representations*, 2020.
- [17] L. Ambrosio, N. Gigli, and G. Savaré, *Gradient flows: in metric spaces and in the space of probability measures*. Springer Science & Business Media, 2008.
- [18] L. Kantorovich, “On translation of mass,” *Doklady Akademii nauk SSSR*, vol. 37, pp. 227–229, 1942.
- [19] R. Flamary, N. Courty, A. Gramfort, M. Z. Alaya, A. Boisbunon, S. Chambon, L. Chapel, A. Corenflos, K. Fatras, N. Fournier, L. Gautheron, N. T. Gayraud, H. Janati, A. Rakotomamonjy, I. Redko, A. Rolet, A. Schutz, V. Seguy, D. J. Sutherland, R. Tavenard, A. Tong, and T. Vayer, “Pot: Python optimal transport,” *Journal of Machine Learning Research*, vol. 22, no. 78, pp. 1–8, 2021. [Online]. Available: <http://jmlr.org/papers/v22/20-451.html>
- [20] G. Mialon, D. Chen, A. d’Aspremont, and J. Mairal, “A trainable optimal transport embedding for feature aggregation and its relationship to attention,” in *ICLR 2021-The Ninth International Conference on Learning Representations*, 2021.
- [21] B. Schölkopf, A. J. Smola, F. Bach *et al.*, *Learning with kernels: support vector machines, regularization, optimization, and beyond*. MIT press, 2002.
- [22] N. Naderializadeh, S. Kolouri, J. F. Comer, R. W. Andrews, and H. Hoffmann, “Set representation learning with generalized sliced-wasserstein embeddings,” *arXiv preprint arXiv:2103.03892*, 2021.
- [23] S. Kolouri, K. Nadjahi, U. Simsekli, R. Badeau, and K. Gustavo, “Generalized sliced wasserstein distances,” in *NeurIPS 2019*, 2019.
- [24] M. E. Sander, P. Ablin, M. Blondel, and G. Peyré, “Sinkformers: Transformers with doubly stochastic attention,” *arXiv preprint arXiv:2110.11773*, 2021.
- [25] A. Vaswani, N. Shazeer, N. Parmar, J. Uszkoreit, L. Jones, A. N. Gomez, Ł. Kaiser, and I. Polosukhin, “Attention is all you need,” in *Advances in neural information processing systems*, 2017, pp. 5998–6008.
- [26] P. A. Knight, “The sinkhorn–knopp algorithm: convergence and applications,” *SIAM Journal on Matrix Analysis and Applications*, vol. 30, no. 1, pp. 261–275, 2008.
- [27] D. Goldfarb and J. K. Reid, “A practicable steepest-edge simplex algorithm,” *Mathematical Programming*, vol. 12, no. 1, pp. 361–371, 1977.
- [28] M. Cuturi, “Sinkhorn distances: Lightspeed computation of optimal transport,” in *Advances in Neural Information Processing Systems (NIPS)*, 2013, pp. 2292–2300.
- [29] D. P. Bertsekas, “Nonlinear programming,” *Journal of the Operational Research Society*, vol. 48, no. 3, pp. 334–334, 1997.
- [30] S. G. Krantz and H. R. Parks, *The implicit function theorem: history, theory, and applications*. Springer Science & Business Media, 2012.

- [31] “Ott toolbox,” <https://ott-jax.readthedocs.io/en/latest/>, released:March 2021.
- [32] M. Cuturi, O. Teboul, J. Niles-Weed, and J.-P. Vert, “Supervised quantile normalization for low rank matrix factorization,” in *International Conference on Machine Learning*. PMLR, 2020, pp. 2269–2279.
- [33] F. Zhang, *The Schur complement and its applications*. Springer Science & Business Media, 2006, vol. 4.
- [34] E. Stiefel, “Methods of conjugate gradients for solving linear systems,” *J. Res. Nat. Bur. Standards*, vol. 49, pp. 409–435, 1952.
- [35] H. Maron, H. Ben-Hamu, N. Shamir, and Y. Lipman, “Invariant and equivariant graph networks,” in *International Conference on Learning Representations*, 2019. [Online]. Available: <https://openreview.net/forum?id=Syx72jC9tm>
- [36] S. Afriat, “Theory of maxima and the method of lagrange,” *SIAM Journal on Applied Mathematics*, vol. 20, no. 3, pp. 343–357, 1971.
- [37] A. Takayama and T. Akira, *Mathematical economics*. Cambridge university press, 1985.
- [38] J. Bradbury, R. Frostig, P. Hawkins, M. J. Johnson, C. Leary, D. Maclaurin, G. Necula, A. Paszke, J. VanderPlas, S. Wanderman-Milne, and Q. Zhang, “JAX: composable transformations of Python+NumPy programs,” 2018. [Online]. Available: <http://github.com/google/jax>
- [39] J. J. Sutherland, L. A. O’Brien, and D. F. Weaver, “Spline-fitting with a genetic algorithm: A method for developing classification structure- activity relationships,” *Journal of chemical information and computer sciences*, vol. 43, no. 6, pp. 1906–1915, 2003.
- [40] G. King and L. Zeng, “Logistic regression in rare events data,” *Political analysis*, vol. 9, no. 2, pp. 137–163, 2001.
- [41] J. Feydy, T. Séjourné, F.-X. Vialard, S.-i. Amari, A. Trounev, and G. Peyré, “Interpolating between optimal transport and mmd using sinkhorn divergences,” in *Proceedings of the Twenty-Second International Conference on Artificial Intelligence and Statistics*, ser. Proceedings of Machine Learning Research, K. Chaudhuri and M. Sugiyama, Eds., vol. 89. PMLR, 16–18 Apr 2019, pp. 2681–2690. [Online]. Available: <http://proceedings.mlr.press/v89/feydy19a.html>
- [42] J. MacQueen *et al.*, “Some methods for classification and analysis of multivariate observations,” in *Proceedings of the fifth Berkeley symposium on mathematical statistics and probability*, vol. 1, no. 14. Oakland, CA, USA, 1967, pp. 281–297.
- [43] D. Arthur and S. Vassilvitskii, “k-means++: The advantages of careful seeding,” Stanford, Tech. Rep., 2006.
- [44] U. Von Luxburg, “A tutorial on spectral clustering,” *Statistics and computing*, vol. 17, no. 4, pp. 395–416, 2007.
- [45] T. N. Kipf and M. Welling, “Semi-supervised classification with graph convolutional networks,” in *International Conference on Learning Representations (ICLR)*, 2017.
- [46] D. Pollard, “Quantization and the method of k-means,” *IEEE Transactions on Information theory*, vol. 28, no. 2, pp. 199–205, 1982.
- [47] G. D. Canas and L. A. Rosasco, “Learning probability measures with respect to optimal transport metrics,” in *Proceedings of the 25th International Conference on Neural Information Processing Systems-Volume 2*, 2012, pp. 2492–2500.

- [48] K. M. Borgwardt, C. S. Ong, S. Schönauer, S. Vishwanathan, A. J. Smola, and H.-P. Kriegel, “Protein function prediction via graph kernels,” *Bioinformatics*, vol. 21, no. suppl_1, pp. i47–i56, 2005.
- [49] C. Morris, N. M. Kriege, F. Bause, K. Kersting, P. Mutzel, and M. Neumann, “Tudataset: A collection of benchmark datasets for learning with graphs,” in *ICML 2020 Workshop on Graph Representation Learning and Beyond (GRL+ 2020)*, 2020. [Online]. Available: www.graphlearning.io
- [50] J. Godwin*, T. Keck*, P. Battaglia, V. Bapst, T. Kipf, Y. Li, K. Stachenfeld, P. Veličković, and A. Sanchez-Gonzalez, “Jraph: A library for graph neural networks in jax.” 2020. [Online]. Available: <http://github.com/deepmind/jraph>
- [51] M. Hessel, D. Budden, F. Viola, M. Rosca, E. Sezener, and T. Hennigan, “Optax: composable gradient transformation and optimisation, in jax!” 2020. [Online]. Available: <http://github.com/deepmind/optax>
- [52] T. Hennigan, T. Cai, T. Norman, and I. Babuschkin, “Haiku: Sonnet for JAX,” 2020. [Online]. Available: <http://github.com/deepmind/dm-haiku>
- [53] F. Errica, M. Podda, D. Bacciu, and A. Micheli, “A fair comparison of graph neural networks for graph classification,” in *Proceedings of the 8th International Conference on Learning Representations (ICLR)*, 2020.
- [54] D. P. Kingma and J. Ba, “Adam: A method for stochastic optimization,” in *ICLR (Poster)*, 2015. [Online]. Available: <http://arxiv.org/abs/1412.6980>
- [55] C. Zhang, S. Bengio, M. Hardt, B. Recht, and O. Vinyals, “Understanding deep learning requires rethinking generalization,” in *5th International Conference on Learning Representations, ICLR 2017, Toulon, France, April 24-26, 2017, Conference Track Proceedings*. OpenReview.net, 2017.
- [56] M. Cuturi and D. Avis, “Ground metric learning,” *The Journal of Machine Learning Research*, vol. 15, no. 1, pp. 533–564, 2014.
- [57] M. Heitz, N. Bonneel, D. Coeurjolly, M. Cuturi, and G. Peyré, “Ground metric learning on graphs,” *Journal of Mathematical Imaging and Vision*, vol. 63, no. 1, pp. 89–107, 2021.
- [58] F. Wang and L. J. Guibas, “Supervised earth mover’s distance learning and its computer vision applications,” in *European Conference on Computer Vision*. Springer, 2012, pp. 442–455.
- [59] G. Zen, E. Ricci, and N. Sebe, “Simultaneous ground metric learning and matrix factorization with earth mover’s distance,” in *2014 22nd International Conference on Pattern Recognition*. IEEE, 2014, pp. 3690–3695.